Enhanced spin pumping near a magnetic ordering transition

Behrouz Khodadadi,[1] Jamileh Beik Mohammadi,[1] Claudia Mewes,[1] Tim Mewes,[1]
M. Manno,[2] C. Leighton,[2] and Casey W. Miller[3,4,*]

[1]*Department of Physics and Astronomy, MINT Center, The University of Alabama, Tuscaloosa, Alabama 35487, USA*
[2]*Department of Chemical Engineering and Materials Science, University of Minnesota, Minneapolis, Minnesota 55455, USA*
[3]*School of Chemistry and Materials Science, Rochester Institute of Technology, Rochester, New York 14623, USA*
[4]*Department of Physics, University of Gothenburg, 412 96 Gothenburg, Sweden*

(Received 17 May 2017; revised manuscript received 21 July 2017; published 25 August 2017)

We study the temperature-dependent static and dynamic magnetic properties of polycrystalline bilayers of permalloy ($Ni_{80}Fe_{20}$, or Py) and gadolinium (Gd) bilayers using DC magnetometry and broadband ferromagnetic resonance. Magnetometry measurements reveal that the 3-nm-thick Gd layers undergo a magnetic ordering transition below 100 K, consistent with finite size suppression of their Curie temperature. Upon cooling below this Gd ordering temperature, ferromagnetic resonance spectroscopy reveals a sharp increase in both the gyromagnetic ratio (γ) and effective Gilbert damping parameter (α_{eff}) of the neighboring Py layers. The increase of γ is attributed to the onset of strong antiferromagnetic coupling between the Gd and Py layers as the Gd orders magnetically. We argue that the increase of α_{eff}, on the other hand, can be explained by spin pumping into the rare-earth layer when taking into account the increase of γ, the decrease of the Gd spin diffusion length as it orders, and, most significantly, the corresponding increase of the Py/Gd interfacial spin mixing conductance in the vicinity of the magnetic ordering transition. We propose that these observations constitute a qualitative confirmation of a recent theoretical prediction of spin sinking enhancement in this situation.

DOI: 10.1103/PhysRevB.96.054436

I. INTRODUCTION

Magnetization dynamics of magnetic multilayers, in addition to being an interesting fundamental research subject in its own right, also has many implications for the design and development of spintronic devices. While the Landau-Lifshitz-Gilbert equation of motion [1,2] has been very successful in describing magnetization dynamics in ferromagnet-containing systems, the origin and underpinnings of the damping parameter α continue to be a major focus of current research [3]. A number of different physical mechanisms have the functional form of the damping term introduced by Gilbert, including, for example, spin-orbit relaxation [4,5], magnon-phonon relaxation [6], eddy current damping [7–9], and spin pumping [10–12]. In magnetic multilayers and heterostructures, spin pumping is often found to be one of the dominant contributions to magnetic relaxation [13,14]. Because spin pumping enables the generation of pure spin currents in normal metals adjacent to ferromagnets [15,16], which in turn can be detected using the inverse spin Hall effect [17–20], this relaxation mechanism has been studied in great detail in ferromagnet/nonmagnetic metal systems. Recent theoretical work has suggested a new avenue of research in this general area by predicting that the interfacial spin-mixing conductance, and thus magnetic relaxation, can be significantly enhanced when spin pumping is performed not into a conventional nonmagnetic metal, but rather into a metallic system undergoing a paramagnet to ferromagnetic transition on cooling [21]. This essentially expands this research into the situation where spin pumping occurs into a metal with strong ferromagnetic spin correlations, which is the subject of this paper.

Broadband ferromagnetic resonance (FMR) is a technique that has been widely used to investigate the magnetic relaxation mechanisms in ferromagnetic thin films, as well as spin pumping into adjacent nonmagnetic layers [22–26]. In this work, we employ FMR to probe the above mentioned situation of spin pumping into a layer undergoing a ferromagnetic ordering transition by studying transition metal/rare earth bilayers. Such a multilayer system is one natural choice to realize this situation, using the transition metal as a relatively simple, low damping, high Curie temperature ferromagnet, and the rare earth as a high atomic number, low Curie temperature adjacent layer. Specifically, we employ here bilayers of permalloy ($Ni_{80}Fe_{20}$, or Py) and gadolinium (Gd) bilayers with Py thicknesses of 5 and 10 nm, and a Gd thickness of only 3 nm, thus suppressing the rare-earth ordering temperature by finite size effects. By studying the temperature dependence of the FMR of the Py in these bilayers, we are thus able to investigate the influence of the magnetic ordering transition in the Gd [27,28] on the magnetization dynamics and relaxation in the Py. We find that the Gd paramagnetic to ferromagnetic transition indeed has a strong influence on the gyromagnetic ratio and effective Gilbert damping parameter of Py. Clear enhancement is seen in both quantities across the transition, which we interpret in terms of strong antiferromagnetic interlayer coupling, as well as the critical temperature dependence of the Py/Gd spin mixing conductance and Gd spin diffusion length. These results are then compared to recent theoretical predictions, which we believe we qualitatively confirm.

II. EXPERIMENTAL DETAILS

The Py/Gd bilayers were deposited on Si/a-SiO_x substrates using a multi-source RF magnetron sputtering system with a base pressure better than 2×10^{-8} Torr. The layers were sequentially sputtered, with no break in vacuum, in 3 mTorr of ultra-high-purity Ar gas at ambient temperature. This was done

*Corresponding author: cwmsch@rit.edu

from a $Ni_{80}Fe_{20}$ target at a deposition rate of 0.044 nm/s, and from an elemental Gd target at a deposition rate of 0.057 nm/s. We note that the growth of high quality Gd in this sputter tool has been previously accomplished [29], with protocols published elsewhere [30]. The specific structures grown here were Py(5 or 10 nm)/Gd(3 nm)/Al(5 nm). The Al capping layer was chosen as an oxidation barrier as any remaining unoxidized Al metal should not significantly influence the magnetization dynamics under investigation, due to the low spin-orbit coupling and relatively large spin diffusion length of Al. With similar concerns in mind, we also avoided often used seed layer metals such as Ta, as those could serve as unintentional spin sinks, and thus a source of additional magnetization damping.

In-plane magnetometry characterization of these bilayers was performed between 5 and 400 K, in fields up to 90 kOe, using a Quantum Design Physical Property Measurement System (PPMS) equipped with a vibrating sample magnetometer (VSM) option. Some out-of-plane measurements were also performed using a Quantum Design Magnetic Property Measurement System (MPMS) XL7 SQUID magnetometer. In that case, samples were mounted using concentric self-tightening polyethylene straws to minimize background signals and artifacts [31]. For both orientations of the magnetic field, samples were cooled in a +90 kOe magnetic field, and high-field linear background subtraction was applied to remove contributions from the holder and substrate. Importantly, the magnetization values reported below are all based on the *combined* nominal thickness of the Py and Gd, i.e., we plot the moment per *total* volume of Py and Gd layers.

Temperature-dependent broadband FMR measurements were carried out using a custom designed setup capable of measuring in the frequency range 1–40 GHz [32–34]. The raw FMR spectra were fit using a derivative of a Lorentzian line shape [35] in order to determine the resonance field (H_{res}) and the peak-to-peak linewidth (ΔH) as functions of frequency and temperature. As recently shown by Shaw *et al.* [36], broadband FMR is useful for reducing experimental error margins when determining gyromagnetic ratios and damping parameters.

III. RESULTS AND ANALYSIS

In the sections below, we provide first the results of magnetometry characterization, followed by temperature-dependent FMR measurements.

A. Magnetometry

In-plane magnetization hysteresis loops were first measured at temperatures T between 10 and 400 K, in magnetic fields up to 90 kOe. Hysteresis loops of the Py(10 nm)/Gd(3 nm) bilayer taken at 10, 30, 40, 50, 60, and 200 K are shown in Fig. 1. The magnetic response is seen to be quite complex, due to the superposition of Gd finite size effects and strong Py-Gd interlayer coupling, which is known to generate high saturation fields [27,37,38] antiferromagnetic interactions, and noncollinear spin states [39]. Specifically, Py(10 nm)/Gd(3 nm) bilayers exhibit soft ferromagnetic behavior above 200 K with negligible coercivity and 95% of the saturation magnetization M_s being reached in only 1 kOe. Below 100 K,

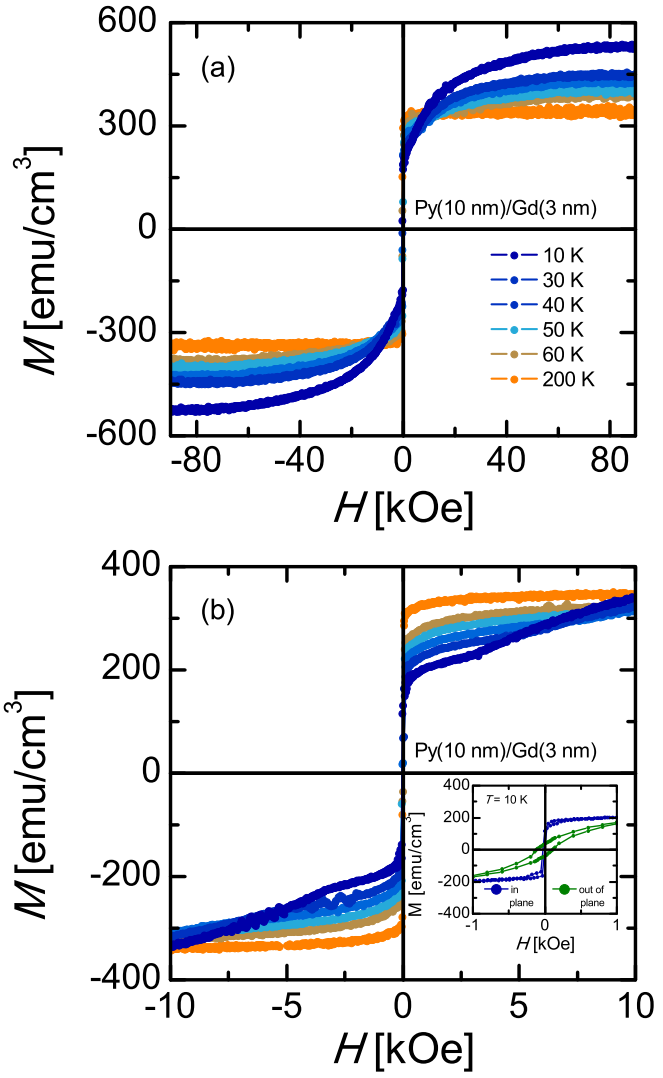

FIG. 1. Representative in-plane hysteresis loops of the Py(10 nm)/Gd(3 nm) bilayer at multiple temperatures. Magnetization was determined using the *combined* thickness of the Py and Gd layers, as also emphasized in the text. Magnetic field sweeps up to 90 kOe are show in (a), while expanded 10 kOe magnetic field sweeps are shown in (b). (Inset) Comparison of the film's magnetic response to in-plane and out-of-plane magnetic fields at 10 K.

however, the soft, low-field character remains, but new features appear. First, a high-field component emerges [Fig. 1(a)], with the apparent M_s rising by more than 50% as T is decreased to 10 K. We ascribe this to the onset of thermally stable ferromagnetism in the Gd, adding to the existing soft ferromagnetism of Py. While bulk Gd has a Curie temperature near ambient (∼292 K) [40,41], finite size effects are well-known in general, and specifically in Gd films, multilayers, and nanoparticles, and can produce ordering temperatures well below 300 K [27,38,42]. The second noticeable feature is that the additional low T magnetization saturates quite slowly with increasing field. In the Py(10 nm)/Gd(3 nm) bilayer shown in Fig. 1(a), saturation is reached only after applying 80 kOe at 10 K. This is yet more pronounced in the Py(5 nm)/Gd(3 nm) case (data not shown), to the point that 90 kOe was not

sufficient to completely saturate the sample at low T. Thirdly, the rise in M_s on cooling below 100 K is also accompanied by distinct changes in the low-field behavior (below 10 kOe). As best seen in Fig. 1(b), the low-field magnetization in fact decreases monotonically on cooling, the magnetization at/1 kOe, for example, $M_{1\,\mathrm{kOe}}$, falls by 37% from 100 to 10 K. Closer examination of the 10-K data further reveals rapid apparent saturation at low fields, followed by a kink at ∼3 kOe, then a gradually increasing magnetization until true saturation is achieved near 80 kOe. We note additionally at this point that while in-plane anisotropy clearly dominates, out-of-plane magnetization measurements at 10 K do reveal both finite coercivity (∼120 Oe) and remanence [inset to Fig. 1(b)]. This indicates a weak out-of-plane component to the anisotropy.

We interpret the behavior displayed in Fig. 1 in terms of antiferromagnetic coupling between Py and Gd. This has been previously observed in various transition metal /rare-earth systems, including Fe/Gd [43], Fe/Gd-Fe [44], Co/Gd [45,46], and even Py/Gd [39], the system studied here. Using the 10-K field sweep in Fig. 1 to illustrate this, as H approaches 90 kOe, the magnetizations of the Gd and Py layers are apparently aligned near parallel to each other, and to the magnetic field. (We note that whether true saturation is achieved in 90 kOe is not completely clear here, as noncollinear states due to competition between antiferromagnetic coupling and Zeeman energies can result in very large saturation fields in Py/Gd, with spin angles varying over larger distances than our film thicknesses [39]). As the applied field is decreased, the antiferromagnetic coupling between the Py and Gd causes the Gd spins to rotate progressively away from the Py magnetization, which remains predominantly aligned with the field. This leads to a reduction of the low-field magnetization upon cooling, i.e., as the Gd becomes ordered and the antiferromagnetic coupling dominates [Fig. 1(b)]. In this picture, the kink observed near 3 kOe at 10 K [Fig. 1(b)] is likely a spin-flop-type transition, as seen in Fe/Gd-Fe [44] and Co/Gd multilayers [46].

In order to further elucidate the antiferromagnetic coupling in these Py/Gd bilayers, Fig. 2 plots M_s and $M_{1\,\mathrm{kOe}}$ for both the Py(10 nm)/Gd(3 nm) and Py(5 nm)/Gd(3 nm) samples. As we could not clearly saturate the Py(5 nm)/Gd(3 nm) bilayer in 90 kOe, we plot the maximum magnetization (M_{max}) for this sample, as an approximation to M_s. These plots clearly reflect the two main conclusions from the magnetometry discussed above: ferromagnetic order in the Gd layers sets in around 60–80 K, and antiferromagnetic coupling between the Py and Gd simultaneously emerges. The former is reflected in the clear increase in M_{s} (or M_{max}) on cooling, while the latter is indicated by the corresponding decrease in $M_{1\,\mathrm{kOe}}$.

A quantitative analysis reveals further interesting features, particularly with respect to the absolute magnetization values. The bulk M_s values of Py and Gd are ∼800 emu/cm^3 at $T = 290$ K [41], and ∼2100 emu/cm^3 when $T < 10$ K [27,37,40], respectively, resulting in a total averaged expected M_s of 1100 emu/cm^3 for the Py(10 nm)/Gd(3 nm) bilayer at 10 K. Reference to Fig. 2(a) immediately reveals that these bilayers have significantly reduced M_s in comparison to these simple expectations. This is true even at high T, above the Gd ordering temperature, with the 400-K M_s values for the Py(10 nm)/Gd(3 nm) and Py(5 nm)/Gd(3 nm) bilayers being

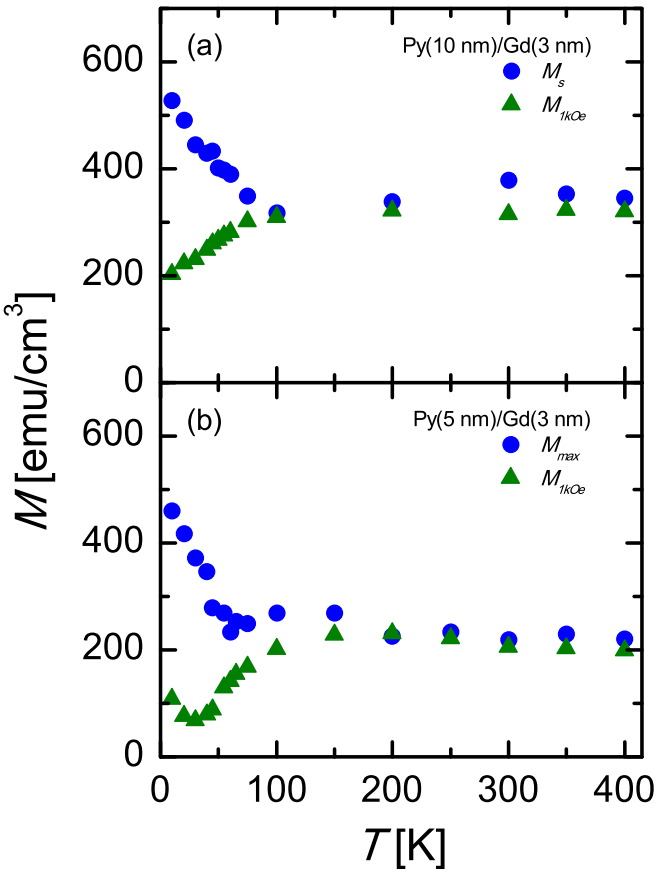

FIG. 2. Temperature dependence of the saturation magnetization (M_s) and the magnetization at 1 kOe ($M_{1\,\mathrm{kOe}}$) for the (a) Py(10 nm)/Gd(3 nm) and (b) Py(5 nm)/Gd(3 nm) bilayers. As discussed in the text, the Py(5 nm)/Gd(3 nm) bilayer did not completely reach saturation even in 90 kOe, leading us to report the maximum magnetization achieved (M_{max}) rather than M_s.

44% and 56% lower, respectively, than expectations for Py alone. This reduction in magnetization is maintained at low T, with the 3-nm Gd layers displaying magnetizations about 60%–70% lower than simple bulk estimates. Considering possible explanations for this, trivial possibilities such as miscalibration of magnetometers or deposition rates were ruled out; these would need to involve ∼50% inaccuracies, far above our estimates. Another possibility is ineffective Al capping, leading to partial oxidation of the underlying magnetic bilayers. We stress, however, that we did not detect any signatures (including exchange bias) of the presence of Ni-O, Fe-O, and/or Gd-O phases. A third possibility, at least partially supported by prior work, is that some fraction of the Gd layer has a significantly proximity-enhanced Curie temperature, and is antiferromagnetically coupled to the Py layer even at 400 K, thus reducing the apparent M_s. Strong proximity effects enhancing the Curie temperature of Gd layers in contact with transition metal layers have in fact been clearly elucidated in systems such as Fe/Gd [47] and $Ni_{1-x}Fe_x$/Gd [48]. A recent x-ray magnetic circular dichroism (XMCD) study of $Ni_{1-x}Fe_x$/Gd multilayers by Ranchal *et al.*, for example, showed that this interfacial Gd layer is 1 – 2.5-nm thick, aligned antiparallel to the $Ni_{1-x}Fe_x$ magnetization [48],

with an enhanced ordering temperature of up to 550 K. If we assume that our observed reduced M_s at high T is associated with such an ordered interfacial Gd layer, we estimate this layer to be ∼1.6-nm and 0.9-nm thick for the Py(10 nm)/Gd(3 nm) and Py(5 nm)/Gd(3 nm) bilayers, respectively. This matches very well with Ranchal *et al.*'s observations. This would result in Gd near the Al cap layer of the heterostructure (i.e., far from the Py interface) that is magnetically disordered at high T, with 1.4-nm thickness in the Py(10 nm)/Gd(3 nm) bilayer, and 2.1-nm thickness in the Py(5 nm)/Gd(3 nm) bilayer. The increase in M_s (or $M_{\max}$) on cooling below 100 K would then be due to the ferromagnetic ordering of this "cap-side" Gd (still antiferromagnetically coupled to the Py). Assuming that the rise in M_s (or $M_{\max}$) at 10 K is indeed due to the onset of ferromagnetism in this noninterfacial Gd layer, its thickness can be estimated to be ∼1.1 nm for the Py(10 nm)/Gd(3 nm) case, and 0.8 nm for the Py(5 nm)/Gd(3 nm) case, reasonably consistent with the above arguments. We thus consider this a possibility in this case, although this would require very strong antiferromagnetic coupling between the interfacial Gd layer and the Py, and a Gd Curie point enhanced well above 400 K. Future work with element-resolved techniques such as XAS and XMCD could potentially test this.

B. Ferromagnetic resonance measurements

Having characterized the static magnetic response of these Py/Gd bilayers across the Gd ordering temperature, dynamic characterization was performed via temperature-dependent FMR. These FMR results show significant temperature dependence to both the Py gyromagnetic ratio and the effective damping parameter, which we treat below in turn. Due to the significant broadening of the resonance with decreasing temperatures, we were limited in our ability to measure ferromagnetic resonance spectra to temperatures above 65 and 50 K for the 5-nm and 10-nm Py films, respectively. We also note that no discernible resonance features were observed at lower temperatures, down to 10 K.

1. Gyromagnetic ratio

As shown in the inset to Fig. 3(a), the Py FMR spectra are strongly temperature dependent at a given frequency (in this case, 10 GHz), both the resonance field and linewidth changing substantially on cooling. Figure 3(a) shows that the relationship between resonance field and frequency f follows the usual Kittel behavior at all temperatures in these Py/Gd bilayers. Least square fits using Kittel's formula [49],

$$f = \gamma' \sqrt{H(H + 4\pi M_{\text{eff}})}, \tag{1}$$

where used to extract the gyromagnetic ratio $\gamma' = \frac{g\mu_B}{h}$ and the effective magnetization M_{eff} at each T. Here, g is the g factor, μ_B the Bohr magneton, and h the Planck constant. As evident from the fit curves shown in Fig. 3(a), Eq. (1) provides an excellent description of the experimental data over the entire f range. Although the significant broadening of the resonance with decreasing T [see inset to Fig. 3(a)] limited our ability to measure spectra at the lowest T, as shown in Fig. 3(b), we find a considerable increase in the gyromagnetic ratio on cooling, particularly below about 50–70 K. In terms of g factors, at 300 K, we find $g = 2.116$ for the 10 nm and $g = 2.141$ for the 5 nm Py, which are both somewhat larger than the bulk value of $g_{\text{NiFe,bulk}} = 2.109$ determined by Shaw *et al.* using similar broadband FMR techniques [36]. We note that the increase is stronger for the thinner NiFe film, consistent with an interfacial origin of the enhancement.

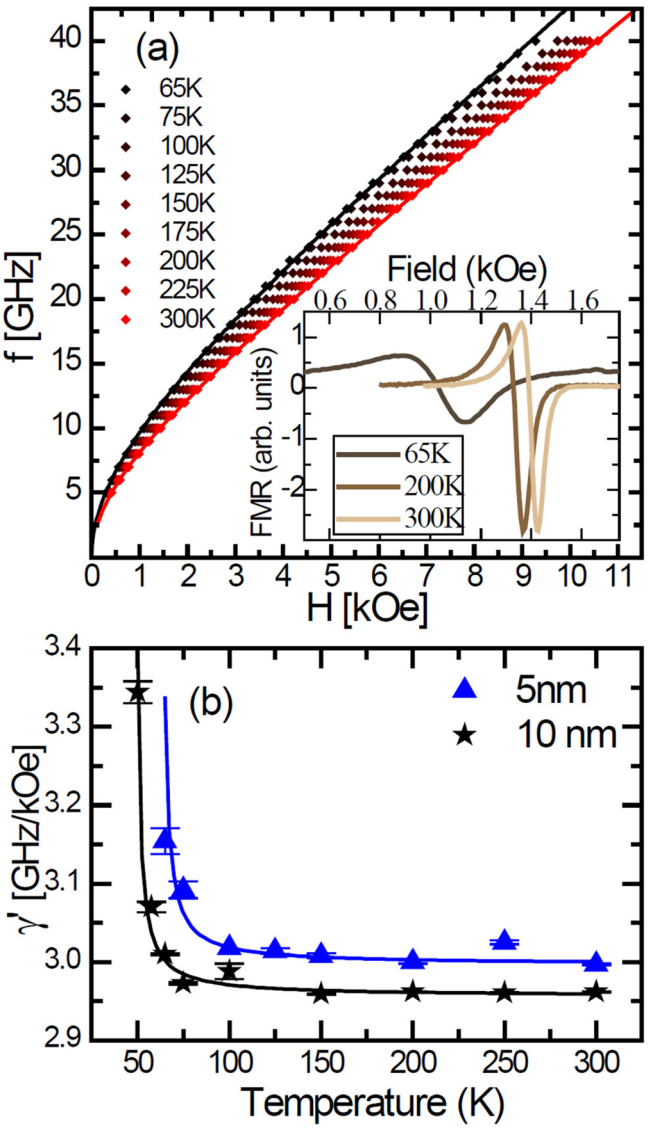

FIG. 3. (a) FMR frequency as a function of resonance field for the Py(5 nm)/Gd(3 nm) bilayer at various temperatures; solid lines are fits to the Kittel equation at 65 and 300 K as examples. (Inset) Example FMR spectra at 10 GHz and three representative temperatures. (b) Temperature dependence of the gyromagnetic ratio for 5-nm and 10-nm Py films capped with 3 nm of Gd.

The apparent divergence of the gyromagnetic ratio at low T resembles the increase of this ratio seen in ferrimagnetic alloys near a compensation point [50–53]. The effective gyromagnetic ratio for ferrimagnetic alloys is the ratio of the net magnetization to the net angular momentum, S [51]. In the case of antiferromagnetic coupling between two sublattices (or in the present case between Py and Gd layers) the net angular momentum is $S = M_{\text{Py}}/\gamma'_{\text{Py}} - M_{\text{Gd}}/\gamma'_{\text{Gd}}$, where the subscripts indicate the contributions from the individual layers. In this case, where M_{Py} is essentially independent of

temperature, an increasing M_{Gd} with decreasing temperature reduces the net angular momentum. As S approaches zero at the angular momentum compensation temperature, the effective gyromagnetic ratio thus diverges. No such divergence of the gyromagnetic ratio would be expected in a system with ferromagnetic coupling between layers. As the magnetometry measurements in Sec. III A clearly revealed antiferromagnetic coupling between the Py/Gd bilayers, this therefore qualitatively explains the strong T dependence of γ'. The temperatures for the divergence in γ' indeed roughly correspond to the increases in M_s in Figs. 2(a) and 2(b).

One limitation to the above is that an underlying assumption used to derive Eq. (1) is that the ferromagnet is saturated. However, the magnetometry data indicate that the low-T magnetization in these bilayers still varies with applied magnetic field, even for the largest fields in the FMR experiments, indicating that the samples are not fully saturated at low T. While it is generally difficult to obtain closed-form expressions for the ferromagnetic resonance condition in unsaturated samples, one can obtain valuable insight by simply assuming that the effective magnetization increases linearly with the applied field H [see Fig. 1(b)], i.e.,

$$M_{\text{eff}} = M_{\text{eff}}(H) = M_{\text{eff},0} + qH, \text{ with } q \geqslant 0. \tag{2}$$

The parameter q is related to the field-dependent net magnetization as the two independent layers' magnetizations align with increasing field, a consequence of the antiferromagnetic coupling between the Py and Gd. Using the linearized model captured by Eq. (2) one obtains a modified Kittel equation:

$$f = \tilde{\gamma}'\sqrt{H(H + 4\pi\tilde{M}_{\text{eff}})}, \tag{3}$$

where the modified effective gyromagnetic ratio $\tilde{\gamma}'$ and effective magnetization $\tilde{M}_{\text{eff}}$ are defined as

$$\tilde{\gamma}' = \gamma'\sqrt{1 + 4\pi q}, \quad \tilde{\gamma}' \geqslant \gamma' \tag{4}$$

$$\tilde{M}_{\text{eff}} = \frac{M_{\text{eff},0}}{1 + 4\pi q}, \quad \tilde{M}_{\text{eff}} \leqslant M_{\text{eff},0}. \tag{5}$$

Equation (3) has the same functionality as the Kittel equation, which explains the excellent fit to the experimental data in Fig. 3(a), despite the lack of saturation. While more detailed information would be needed to develop a fully quantitative model, the simplified model resulting in Eq. (4), taken together with the magnetometry data discussed earlier, shows that the gyromagnetic ratio $\tilde{\gamma}'$ extracted using the Kittel equation can be expected to be systematically larger than the intrinsic value γ' if the effective magnetization probed by FMR increases with the applied field. While achieving an exact deconvolution of the factors that contribute to the observed increase of the gyromagnetic ratio with decreasing T is beyond the scope of this work, we simply point out that antiferromagnetic coupling between the NiFe and Gd layers is the essential element. This is true for both the picture based on a compensation point of the net angular momentum, and for the field-dependent effective magnetization model.

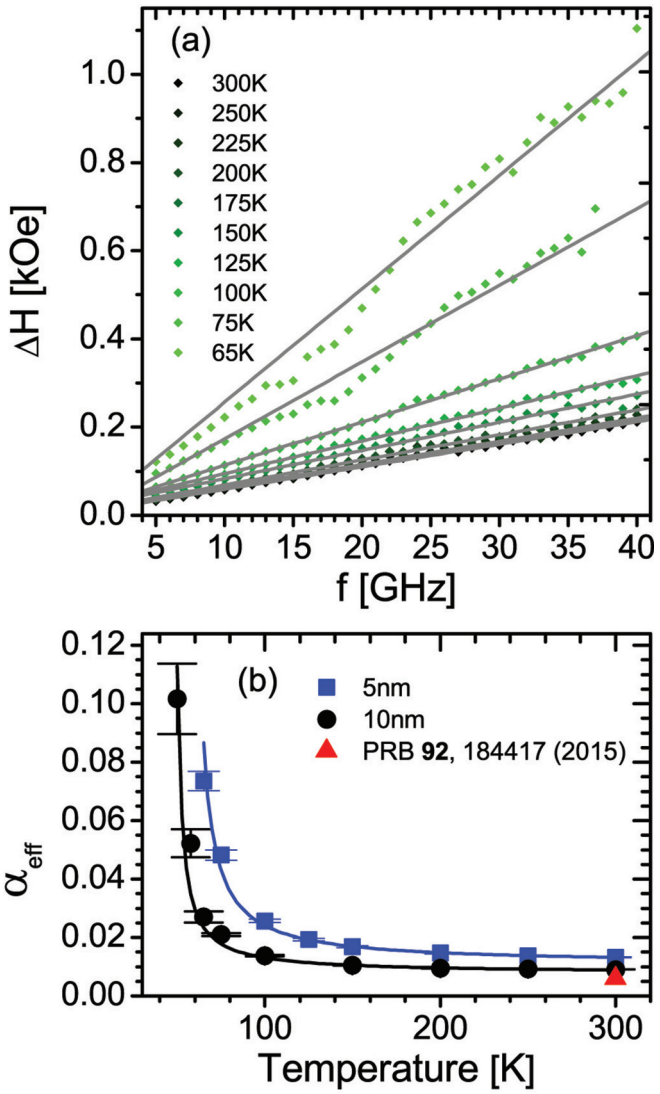

FIG. 4. (a) FMR linewidth as a function of frequency for Py(5 nm)/Gd(3 nm) at various temperatures. Lines are fits to the experimental data used to extract the effective Gilbert damping parameter. (b) Temperature dependence of the effective Gilbert damping parameter for 5-nm and 10-nm Py films capped with 3 nm of Gd. The red triangle indicates the intrinsic damping parameter for Py thin films at room temperature [54].

2. Damping parameter

Figure 4(a) reveals that there also exist strong temperature and frequency dependencies of the FMR linewidth. In the case of Gilbert-type relaxation of the magnetization, the isothermal frequency dependence of the linewidth is expected to be given by [2]

$$\Delta H = \Delta H_0 + \frac{2}{\sqrt{3}}\frac{\alpha_{\text{eff}}}{\gamma'} f, \tag{6}$$

where the slope is proportional to the effective damping parameter α_{eff}, and the zero-frequency offset ΔH_0 is typically associated with inhomogeneities; ΔH_0 was less than 2 Oe for these samples. Using the gyromagnetic ratio extracted from the Kittel analysis at each temperature [Fig. 3(b)], fits to the data

in Fig. 4(a) using Eq. (6) yield the temperature-dependent α_{eff} shown in Fig. 4(b). For both bilayers, the effective damping parameter increases significantly on cooling, particularly around 50–70 K, similar to what was observed for the gyromagnetic ratio. Note, however, that the change in α_{eff} is roughly an order of magnitude between 300 K and the lowest measurable temperatures [Fig. 4(b)], which is much more significant than the 10% increase seen in the gyromagnetic ratio [Fig. 3(b)]. Overall the effective damping parameter is larger for the thinner Py layer, which is consistent with the Gd ordering affecting the Py spin dynamics across the interface.

As discussed in Sec. I, spin pumping is known to contribute to the magnetic relaxation of ferromagnetic films in proximity to normal metal films, or other ferromagnetic films [10,11,13]. Given this, and the fact that the T dependence of the effective damping parameter in these Py/Gd bilayers [Fig. 4(b)] exhibits clear similarities to the T dependence shown in Fig. 2, we now consider the possibility that spin pumping into the Gd is central to our observed damping enhancements. We note immediately that while the T-dependent increase in the gyromagnetic ratio will translate into *some* increase in the effective damping parameter, this is simply too small an effect to explain the order of magnitude increase seen in α_{eff}. Spin pumping from the Py into the Gd should also be affected by the change with temperature of the spin diffusion length in the Gd, however, as well as the change of the spin mixing conductance across the Py/Gd interface. These are both expected to be large effects as the Gd undergoes magnetic ordering on cooling, and they are discussed below in turn. We note that the effective damping at room temperature is enhanced compared to established values for Py [54]. However, because for Gd the total magnetic moment is due to spin, with no orbital magnetic moment [55], the enhancement is small, as can be expected due to the lack of spin-orbit interaction in this material [55].

Consider first the contribution to the effective damping parameter related to the T dependence of the Gd spin diffusion length. Based on the theoretical model of spin pumping by Tserkovnyak *et al.* [10,11], the effective Gilbert damping parameter of a ferromagnetic film adjacent to a spin sink can be expressed as the sum of the intrinsic Gilbert damping parameter α_0 and a spin pumping contribution

$$\alpha_{\text{eff}} = \alpha_0 + \left[1 + g^{\uparrow\downarrow}\frac{\tau_{SF}\delta_{SD}/h}{\tanh\left(L/\lambda_{SD}\right)}\right]^{-1}\frac{g g^{\uparrow\downarrow}}{4\pi\mu}, \tag{7}$$

where $g^{\uparrow\downarrow}$ is the interfacial spin mixing conductance, μ is the film's total magnetic moment (the product of magnetization per unit volume, interface area, and film thickness), τ_{SF} is the mean time between spin-flip collisions in the spin sink, δ_{SD} is the effective energy-level spacing of the states that contribute to the spin-flip scattering events, L is the thickness of the adjacent metal layer, and λ_{SD} is the spin diffusion length of that spin sink metal layer. The term $\frac{\tau_{SF}\delta_{SD}/h}{\tanh(L/\lambda_{SD})}$ is commonly referred to as the back-reflection factor. The maximum possible enhancement of the effective Gilbert damping parameter by ordering of an adjacent ferromagnet occurs when this back-reflection factor is zero, yielding

$$\alpha'_{\text{max}} = \frac{g g^{\uparrow\downarrow}}{4\pi\mu}. \tag{8}$$

Approximating the high-temperature spin mixing conductance for our interface at $10\,\text{nm}^{-2}$ [56,57], the maximum damping would then be of the order 0.025 and 0.050 for the 5-nm and 10-nm-thick Py layers, respectively. Given that these α'_{max} estimates are lower by a factor of two than the increases we observed experimentally, this explanation clearly has some limitation. However, it should be emphasized that the existence of proximity-ordered Gd at the Py interface implies that this mechanism likely does contribute to the damping enhancement seen here, throughout the temperature range studied. Note that one can use a more detailed form of Eq. (7), such as the one used in the work by Y. Tserkovnyak *et al.* [12] to express the back-reflection parameter in terms of the Sharvin interface resistance, and eventually the resistance of Gd. However, this does not alter the estimate for the maximum increase in damping expected.

Looking in closer detail, the model associated with Eq. (7) suggests that damping will increase when the spin diffusion length of the spin sink layer is reduced, e.g., below a magnetic ordering transition. Since the spin diffusion length λ_{SD} of a ferromagnetic or normal metal can be described by [58]

$$\lambda_{SD} = \sqrt{\left(1-\beta_f^2\right)\frac{\lambda_{sf}\lambda_t}{6}}, \tag{9}$$

where λ_t is the electron mean free path, λ_{sf} is the spin-flip length (the product of the Fermi velocity and τ_{SF}), and β_f is an asymmetry coefficient related to the spin polarization (which scales as the magnetic order parameter), the temperature dependence of damping should then vary in a manner controlled by the magnetic order parameter [by combining Eqs. (7) and (9)]. This is inconsistent with the data in Fig. 4(b) though, which resembles a divergence at the ordering temperature, as opposed to gradual growth as order develops. The heterogeneity of magnetic ordering of the Gd with both depth and temperature clearly complicates the situation, however; unfortunately, we are aware of no measurements of Gd spin diffusion length in this or simpler situations. Even if we were measuring fully ordered Gd, existing measurements of the spin polarization of Gd suggest that it is not particularly large, which would limit the impact on damping (via β_f). For example, in the pioneering work of Tedrow and Meservey [59] the reported spin polarization of Gd at 0.4 K was only 4.3%, and in temperature dependent spin-polarized photoemission studies of Gd(0001) the measured spin polarization did not exceed 30% even well below the Curie temperature [60]. While these different measurement techniques probe different spin polarizations, all reported values for Gd are low. We therefore expect that this contribution has a relatively minor effect on the temperature dependence of damping.

More consistent with the major features of our data, a recent study by Ohnuma *et al.* [21] offers another mechanism, based on the spin mixing conductance, that could explain the enhanced damping as T approaches the Gd phase transition from above. That work extends an alternative theory of spin pumping first proposed by E. Simanek and B.Heinrich [61] and uses a linear-response theory to clarify the role of spin fluctuations in spin sinking, for a metallic ferromagnet near its

Curie temperature. In this theory, spin pumping is enhanced as T is lowered toward the Curie temperature of the spin sink layer, due to an increase of the spin mixing conductance across the interface. This is caused by the proportionality of the spin mixing conductance to the momentum sum of the imaginary part of the dynamical transverse spin susceptibility in the spin sink layer:

$$g^{\uparrow\downarrow} \propto \sum_k Im\ \chi_k^R(\omega_{\rm rf}), \tag{10}$$

where χ_k^R is the dynamical transverse spin susceptibility and $\omega_{\rm rf}$ is the microwave frequency. This magnetic susceptibility diverges as T is lowered toward the Curie temperature at a standard second-order paramagnetic to ferromagnetic phase transition, as expected for Gd (at least from dc measurements) [62,63]. Thus Eq. (10) suggests that the spin mixing conductance should increase dramatically on cooling as the magnetic ordering temperature is approached. Assuming a small back-reflection term, one would expect the damping parameter to increase with a susceptibilitylike T dependence [from Eqs. (7) and (10)], qualitatively consistent with our data. While the complicated depth- and temperature-dependent ordering of the Gd layer, and the lack of independent data for the spin diffusion length, prevent us from quantitatively determining the two contributions to the T dependence of the damping enhancement in our case, the qualitative features of our data do suggest that the spin mixing conductance is the dominant factor. This is clear from the appearance of (susceptibility-like) divergence of $\alpha_{\rm eff}$ at the Gd ordering temperature, as opposed to (order-parameter-like) gradual growth in $\alpha_{\rm eff}$ on cooling below the Curie temperature, thus providing a qualitative confirmation of the prediction of Ohnuma *et al.* A quantitative test of the exact temperature dependence in Fig. 4(b) would require careful T-dependent measurements of the Gd spin polarization, spin diffusion length, and dynamical spin susceptibility, which is clearly demanding. We note however that the linewidth data shown in Fig. 4(a) deviate from the linear dependence described by Eq. (6), which was used for all datasets to enable a quantitative data analysis with a minimal set of free parameters. These deviations are expected, due to the field dependence of the susceptibility [see Fig. 1(b)] and thus provide further evidence that this mechanism contributes significantly to the observed temperature dependence of the effective damping.

IV. SUMMARY

In summary, we combined temperature-dependent dc magnetometry and broadband ferromagnetic resonance to study Py/Gd bilayers both above and below the temperature at which the Gd orders magnetically. We find finite-size-suppressed Gd ordering temperatures, strong antiferromagnetic coupling between the transition metal and rare earth layers, and evidence of a proximity ordered interfacial component. FMR measurements then reveal clear increases in the gyromagnetic ratio and Gilbert damping parameter of the Py on cooling toward the phase transition temperature of the Gd. The increase in the gyromagnetic ratio can be attributed to the antiferromagnetic coupling between Py and Gd, conceptually similar to compensation points in rare-earth/transition metal alloys. The strong temperature dependence of the effective damping parameter, on the other hand, is caused by enhancement of spin pumping, which we argue to originate from the combined effects of an increasing gyromagnetic ratio, a decreasing Gd spin diffusion length, and most significantly, an increasing spin mixing conductance when approaching the paramagnetic-to-ferromagnetic phase transition of Gd. The latter provides a qualitative confirmation of a recent theoretical prediction.

ACKNOWLEDGMENTS

Work at RIT was supported by NSF-CAREER 1522927. Work at the University of Alabama was supported by NSF-CAREER Award No. 0952929 and by NSF-CAREER Award No. 1452670. Work at the University of Minnesota was supported by NSF under Award No. DMR-1507048. The authors thank T. Eggers for assistance with film deposition, Seungha Yoon for reading the manuscript, and Hiroto Adachi for fruitful discussions.

[1] T. L. Gilbert, Phys. Rev. **100**, 1243 (1955) [Abstract only, not online; full report, Armor Research Foundation Project No. A059, Supplementary Report, May 1, 1956] (unpublished).
[2] T. L. Gilbert, IEEE Trans. Magn. **40**, 3443 (2004).
[3] C. Mewes and T. Mewes, *Handbook of Nanomagnetism* (Pan Stanford, 2015), pp. 71–96.
[4] K. Gilmore, Y. U. Idzerda, and M. D. Stiles, Phys. Rev. Lett. **99**, 027204 (2007).
[5] C. Liu, C. K. A. Mewes, M. Chshiev, T. Mewes, and W. H. Butler, Appl. Phys. Lett. **95**, 022509 (2009).
[6] H. Suhl, IEEE Trans. Magn. **34**, 1834 (1998).
[7] I. D. Mayergoyz, C. Serpico, and Y. Shimizu, J. Appl. Phys. **87**, 5529 (2000).
[8] G. Hrkac, M. Kirschner, F. Dorfbauer, D. Suess, O. Ertl, J. Fidler, and T. Schrefl, J. Appl. Phys. **99**, 08B902 (2006).
[9] E. Martinez, L. Lopez-Diaz, and L. Torres, J. Appl. Phys. **99**, 123912 (2006).
[10] Y. Tserkovnyak, A. Brataas, and G. E. W. Bauer, Phys. Rev. Lett. **88**, 117601 (2002).
[11] Y. Tserkovnyak, A. Brataas, and G. E. W. Bauer, Phys. Rev. B **66**, 224403 (2002).
[12] Y. Tserkovnyak, A. Brataas, G. E. W. Bauer, and B. I. Halperin, Rev. Mod. Phys. **77**, 1375 (2005).
[13] H. Lee, L. Wen, M. Pathak, P. Janssen, P. LeClair, C. Alexander, C. K. A. Mewes, and T. Mewes, J. Phys. D **41**, 215001 (2008).
[14] T. Mewes, R. L. Stamps, H. Lee, E. Edwards, M. Bradford, C. K. A. Mewes, Z. Tadisina, and S. Gupta, IEEE Magn. Lett. **1**, 3500204 (2010).
[15] B. Heinrich, Y. Tserkovnyak, G. Woltersdorf, A. Brataas, R. Urban, and G. E. W. Bauer, Phys. Rev. Lett. **90**, 187601 (2003).
[16] O. Mosendz, G. Woltersdorf, B. Kardasz, B. Heinrich, and C. H. Back, Phys. Rev. B **79**, 224412 (2009).
[17] J. E. Hirsch, Phys. Rev. Lett. **83**, 1834 (1999).
[18] S. Zhang, Phys. Rev. Lett. **85**, 393 (2000).

[19] O. Mosendz, J. E. Pearson, F. Y. Fradin, G. E. W. Bauer, S. D. Bader, and A. Hoffmann, Phys. Rev. Lett. **104**, 046601 (2010).
[20] E. Saitoh, M. Ueda, H. Miyajima, and G. Tatara, Appl. Phys. Lett. **88**, 182509 (2006).
[21] Y. Ohnuma, H. Adachi, E. Saitoh, and S. Maekawa, Phys. Rev. B **89**, 174417 (2014).
[22] B. Heinrich, in *Ultrathin Magnetic Structures II: Measurement Techniques and Novel Magnetic Properties*, edited by B. Heinrich and J. A. C. Bland (Springer, Berlin, Heidelberg, 1994), pp. 195–296.
[23] B. Heinrich, in *Ultrathin Magnetic Structures III: Fundamentals of Nanomagnetism*, edited by J. A. C. Bland and B. Heinrich (Springer, Berlin, Heidelberg, 2005), pp. 143–210.
[24] J. Beik Mohammadi, J. M. Jones, S. Paul, B. Khodadadi, C. K. A. Mewes, T. Mewes, and C. Kaiser, Phys. Rev. B **95**, 064414 (2017).
[25] Y. Cui, J. Lu, S. Schäfer, B. Khodadadi, T. Mewes, M. Osofsky, and S. A. Wolf, J. Appl. Phys. **116**, 073902 (2014).
[26] C. Sterwerf, S. Paul, B. Khodadadi, M. Meinert, J.-M. Schmalhorst, M. Buchmeier, C. K. A. Mewes, T. Mewes, and G. Reiss, J. Appl. Phys. **120**, 083904 (2016).
[27] J. S. Jiang, and C. L. Chien, J. Appl. Phys. **79**, 5615 (1996).
[28] J. S. Jiang, D. Davidović, D. H. Reich, and C. L. Chien, Phys. Rev. Lett. **74**, 314 (1995).
[29] C. W. Miller, D. D. Belyea, and B. J. Kirby, J. Vac. Sci. Technol. A **32**, 040802 (2014).
[30] H. F. Kirby, D. D. Belyea, J. T. Willman, and C. W. Miller, J. Vac. Sci. Technol. A **31**, 031506 (2013).
[31] M. A. Garcia, E. F. Pinel, J. d. l. Venta, A. Quesada, V. Bouzas, J. F. Fernández, J. J. Romero, M. S. M. González, and J. L. Costa-Krämer, J. Appl. Phys. **105**, 013925 (2009).
[32] S. Keshavarz, Y. Xu, S. Hrdy, C. Lemley, T. Mewes, and Y. Bao, IEEE Trans. Magn. **46**, 1541 (2010).
[33] B. Khodadadi, Ph.D. thesis, The University of Alabama, 2016.
[34] N. Pachauri, B. Khodadadi, A. V. Singh, J. B. Mohammadi, R. L. Martens, P. R. LeClair, C. Mewes, T. Mewes, and A. Gupta, J. Magn. Magn. Mater. **417**, 137 (2016).
[35] C. J. Oates, F. Y. Ogrin, S. L. Lee, P. C. Riedi, G. M. Smith, and T. Thomson, J. Appl. Phys. **91**, 1417 (2002).
[36] J. M. Shaw, H. T. Nembach, T. J. Silva, and C. T. Boone, J. Appl. Phys. **114**, 243906 (2013).
[37] G. Scheunert, W. R. Hendren, C. Ward, and R. M. Bowman, Appl. Phys. Lett. **101**, 142407 (2012).
[38] X. G. Liu, D. Y. Geng, Q. Zhang, J. J. Jiang, W. Liu, and Z. D. Zhang, Appl. Phys. Lett. **94**, 103104 (2009).
[39] R. Ranchal, C. Aroca, and E. López, J. Appl. Phys. **100**, 103903 (2006).
[40] H. E. Nigh, S. Legvold, and F. H. Spedding, Phys. Rev. **132**, 1092 (1963).
[41] R. C. O'handley, *Modern Magnetic Materials: Principles and Applications* (Wiley, 2000).
[42] D. Michels, C. E. Krill Iii, and R. Birringer, J. Magn. Magn. Mater. **250**, 203 (2002).
[43] J. L. Prieto, B. B. van Aken, G. Burnell, C. Bell, J. E. Evetts, N. Mathur, and M. G. Blamire, Phys. Rev. B **69**, 054436 (2004).
[44] H. Dohnomae, T. Shinjo, and M. Motokawa, J. Magn. Magn. Mater. **90**, 88 (1990).
[45] J. P. Andrés, L. Chico, J. Colino, and J. M. Riveiro, Phys. Rev. B **66**, 094424 (2002).
[46] J. Colino, J. P. Andrés, J. M. Riveiro, J. L. Martínez, C. Prieto, and J. L. Sacedón, Phys. Rev. B **60**, 6678 (1999).
[47] D. Haskel, G. Srajer, J. C. Lang, J. Pollmann, C. S. Nelson, J. S. Jiang, and S. D. Bader, Phys. Rev. Lett. **87**, 207201 (2001).
[48] R. Ranchal, Y. Choi, M. Romera, J. W. Freeland, J. L. Prieto, and D. Haskel, Phys. Rev. B **85**, 024403 (2012).
[49] C. Kittel, Phys. Rev. **73**, 155 (1948).
[50] C. Mathieu, B. Hillebrands, and D. Raasch, IEEE Trans. Magn. **30**, 4434 (1994).
[51] R. K. Wangsness, Phys. Rev. **91**, 1085 (1953).
[52] R. K. Wangsness, Am. J. Phys. **24**, 60 (1956).
[53] W. Ng, R. F. Soohoo, and R. C. Taylor, J. Appl. Phys. **53**, 2359 (1982).
[54] M. A. W. Schoen, J. M. Shaw, H. T. Nembach, M. Weiler, and T. J. Silva, Phys. Rev. B **92**, 184417 (2015).
[55] W. Bailey, P. Kabos, F. Mancoff, and S. Russek, IEEE Trans. Magn. **37**, 1749 (2001).
[56] A. Ghosh, J. F. Sierra, S. Auffret, U. Ebels, and W. E. Bailey, Appl. Phys. Lett. **98**, 052508 (2011).
[57] M. Zwierzycki, Y. Tserkovnyak, P. J. Kelly, A. Brataas, and G. E. W. Bauer, Phys. Rev. B **71**, 064420 (2005).
[58] B. Jack and P. P. William, Jr., J. Phys.: Condens. Matter **19**, 183201 (2007).
[59] P. M. Tedrow and R. Meservey, Phys. Rev. B **7**, 318 (1973).
[60] D. Li, J. Pearson, S. D. Bader, D. N. McIlroy, C. Waldfried, and P. A. Dowben, Phys. Rev. B **51**, 13895 (1995).
[61] E. Šimánek and B. Heinrich, Phys. Rev. B **67**, 144418 (2003).
[62] J. M. D. Coey, K. Gallagher, and V. Skumryev, J. Appl. Phys. **87**, 7028 (2000).
[63] G. L. F. Fraga, P. Pureur, and L. P. Cardoso, J. Appl. Phys. **107**, 053909 (2010).